Materials Science-Poland, 40(4), 2022, pp. 78-90
http://www.materialsscience.pwr.wroc.pl/
DOI: 10.2478/msp-2022-0046

sciendo

Investigation of aerosol droplets diameter generated in aerosol jet printing

Wojciech Łapa[1,*], Marcin Winnicki[1], Karolina Orłowska[1]

[1]Faculty of Mechanical Engineering, Wrocław University of Science and Technology, 5 Łukasiewicza Street, 50-371 Wrocław, Poland

Aerosol jet printing is a contactless direct-write technique that could be used for the deposition of a variety of materials. First, used for electric paths, the technology was explored for many applications. The substantial part of the process is the generation of aerosols. The size of the droplets and the stability of the process affect the quality of the sprayed lines. This article investigates the diameter of the sprayed droplets, allowing future comparison of the results with sprayed lines. Droplets from ultrasonic and pneumatic generators were sprayed at their outlet on the polyethylene terephthalate (PET) foil. Using a digital microscope and the built-in algorithm, the diameter of the droplets was measured, and the dataset was collected as CSV files and served as a background to the box plot. Scanning electron microscopy (SEM) and atomic force microscopy (AFM) scans were applied to verify the results obtained. The ink parameters used in the process have an influence on the aerosol generation and droplet diameter, whereas the carrier gas pressure has an impact mostly on the droplet diameter. In this case, the aerosol was produced from three types of ink in combination with two generators. For inks with a dynamic viscosity below 6.5 m·Pa^{-1}·s^{-1} a stable range of 5–10 μm droplet diameter was observed. A high-viscosity ink (7.5–10.5 m·Pa^{-1}·s^{-1}) produced droplets with diameter in the range of 6–25 μm. The diameter of the droplet decreased from 7–22 μm to 1–5 μm with a reduction in the dynamic viscosity from 7.5–10.5 m·Pa^{-1}·s^{-1} to 4.5–5.5 m·Pa^{-1}·s^{-1}.

Keywords: *aerosol jet printing, nano ink, aerosol generation, elastic electronics*

1. Introduction

Aerosols are used in various applications, such as humidity control, drug delivery, mass spectrometry, and many more [1, 2]. Each of them requires defined droplet generation. In many cases, the distribution of the droplet size is a key factor. The utilization includes the group of direct write processes with one of the most promising additive manufacturing methods for the fabrication of electronic circuits known as aerosol jet printing (AJP). For aerosol direct write methods, different shapes of nozzles are used to obtain aerodynamic focusing: (i) converging–diverging nozzle, (ii) converging–diverging–converging nozzle, (iii) aerodynamic lensing, and (iv) sheath gas focusing [3]. A specific geometry of the sheath gas focusing nozzle brings an improvement in resolution, miniaturization, and flexibility of the prints in AJP. The graphic illustrating this technique is shown in Figure 1. From the forces that act upon aerosol droplets, the drag and lift forces are distinguished. The directions of the drag forces are parallel to the flow, whereas the lift forces are perpendicular; as a result, different locations of the droplets are caused in the cross section of the canal. Assuming that Brownian movements do not occur and the flow is Poiseuille shear flow, the axial velocity profile is parabolic. The aerosol stream flowing through the canal can be disturbed by two types of perpendicular acting forces: Saffman wall lift forces and shear gradient lift forces. The dominant lift forces in the streamline are the wall effect lift force, where reflection of the stresslet occurring near the wall guides droplets away from the wall. On the contrary, the shear gradient lift force guides the droplets in the direction of the shear gradient, in this case in the direction of the wall [4]. When these forces contradict each other, droplets are located in an equilibrium position inside the canal [5]. Simulations carried out by Cheng et al.

* E-mail: wojciech.lapa@pwr.edu.pl

© Wojciech Łapa et al. 2022. This is an open access article distributed under the Creative Commons Attribution-NonCommercial-NoDerivatives 4.0 License. (http://creativecommons.org/licenses/by-nc-nd/4.0/)

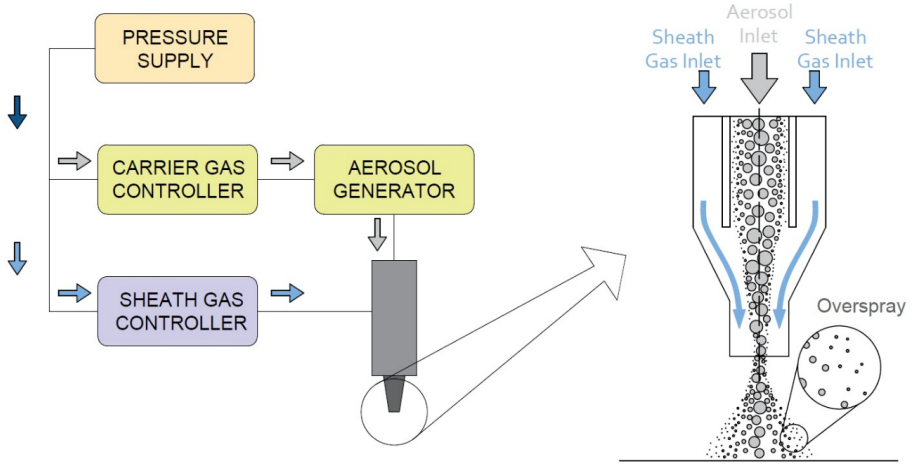


Fig. 1. An illustration of the AJP technique. AJP, aerosol jet printing

[6] indicate that the Saffman wall lift force is crucial for the final location of the droplets. Those with a larger diameter tend to stay near the axis, and those with a smaller diameter are located near the wall. Especially, droplets with diameter of 1 μm or less contribute to spread of the sprayed lines [6]. The Saffman force occurs as a result of the difference in velocities between droplets and carrier gas [7, 8]. After exceeding the nozzle exit, there are no other confinements or effects perpendicular to the flow, which could suggest the key role of the Saffman lift force during overspray formation. Overspray occurs as a result of smaller droplets being out of their aerodynamic focal length region [9]. More monodisperse aerosol reduces the formation of overspray. Furthermore, droplets with a larger diameter (5–10 μm) generate paths with a higher resolution. They have a higher inertia, which allows them to say inside the stream [10]. Finding an optimal range of droplet diameter (DD) plays an essential role during the deposition of high-resolution paths. The literature describes the DD used in the process, but it is not defined whether it is optimal or is the result of the generators used. Certainly, the aerosol parameters should be stable for a long period of time [11].

In the presented study, silver nanoparticle-based inks were used to examine aerosol production by two various aerosol generators, namely, ultrasonic and pneumatic. Overspray is one of the most problematic issues in the AJP process, limiting minimalization of the width of the printed paths, decreasing the height and density of the film, and reducing the deposition efficiency of the process. It should be emphasized that the efficiency of the process depends mainly on the aerosol density entering the mist tube, the aerosol flow rate, and the transport efficiency (droplets that impinge and stick to the tube sidewalls). However, all the specified factors are influenced by the diameter of the aerosol droplets [12]. By combining the properties of the ink with an appropriate aerosol generation technique, it is possible to produce high-quality electronic paths. Therefore, estimation of the optimal DD is necessary to stabilize the printing process and minimize the generation of overspray in printed lines.

2. Literature background

Two techniques used for generating aerosol in AJP are ultrasonic and pneumatic. Researchers propose two theories regarding ultrasonic generation. The first one concludes that atomization is an effect of cavitation, while the second states that static acoustic waves are essential to this process. The theory involving cavitation assumes that the aerosol is produced due to the local pressure, leading to the implosion of the air dissolved in the medium. In the case of acoustic waves, the liq-

uid is excited by ultrasounds, while the appropriate frequency builds up standing capillary waves at the surface. Subsequently, ligament formation occurs and, later, breaks down into separate droplets. Repeatable results would suggest that the static acoustic wave theory is the correct one. On the other hand, some of the research papers constantly advocate cavitation theory. Therefore, several researchers proposed a hybrid model claiming that a standing capillary wave is responsible for droplet generation at the macroscale, while cavitation occurs at the microscale. Nevertheless, an ideal equation for predicting the diameter of the droplet is still missing. Rajan and Pandit [13] in their paper present a broad analysis of the literature. However, the authors do not give a clear answer to the primary question, What truly happens in the aerosol generation process? Empirical research is needed to define the droplet size that reaches the nozzle. The frequency of the wave shapes the width of vibrations that lead to changes in the diameter of the droplet. Higher frequencies produce finer droplets [14]. AJP operates with frequencies ranging from 1.6 MHz to 2.4 MHz, generating droplets within 3–5 μm diameter [11]. The intensity of the process is connected to the amplitude of the sonic wave, which is proportional to the voltage given to the piezoelectric element. The height of the surface waves increases with higher voltage values. The process can be inhibited by a high kinematic viscosity of the ink. The generation of aerosols through this method can be problematic for mediums that have kinematic viscosity values over m/ [15]. The height at which the liquid surface is located above the transducer is also crucial and is defined at the place where the intensity of the process is the maximum. It is worth emphasizing that the formation of a wave with the second peak responsible for the generation of droplets with a larger diameter can occur [16]. It is probably associated with intense vibration of the generator and is not related to frequency. For higher voltage values, this process is more intense. An alternative explanation is the agglomeration of the droplets. Initially, smaller droplets collide and merge with each other [17]. The long-term process leads to the heating of the medium and its drying [11], and consequently introduces problems with the persistence of the stable parameters in time. The overheated medium loses electrostrictive properties [15] and, moreover, experiences surface tension and viscosity modifications [18, 19]. The resulting changes in the ink parameters generate problems with the process stability. Therefore, external cooling is needed.

In pneumatic generators, ligaments are developed by the gas flow tearing off the fraction of liquid. The key parameters are the flow rate and the dependent pressure. Similarly to spray nozzles, the geometry of the generator is crucial as it affects the flow rate in the aerosol formation region. The difference between the velocity of the velocity of the gas and the liquid causes droplet separation after the stagnation pressure. It is defined as $\rho g(v)$, where v is the velocity difference. The diameter of the droplets decreases as the velocity difference increases [20]. It occurs as a consequence of the development of longer and narrower ligaments.

There are two basic laws that describe the atomization process, namely, the Weber capillary law and Reynolds' viscosity law. The interaction between both laws is described with a dimensionless Ohnesorge number by eliminating velocity [21].

The Reynolds number is expressed as:

$$Re = ua\rho/\mu, \tag{1}$$

where u is the characteristic velocity, a is the characteristic dimension, ρ is the density and μ is the dynamic viscosity of the ink.

The Weber number relates inertia to surface tension and is expressed as:

$$We = u^2\rho a/\sigma, \tag{2}$$

where σ is the surface tension of the ink.

The Ohnesorge number is expressed as:

$$Oh = \sqrt{We}/Re = \mu/\sqrt{\sigma\rho a}. \tag{3}$$

3. Experimental

The inks used in the study are commercially available silver nanoparticles suspended in solvent, mostly tetradecane or a mixture of ethanol and glycol (Amepox Microelectronics, Ltd., Łódź,

Table 1. Properties of the inks

Ink	Dynamic viscosity [m·Pa·s]	Surface tension [dynes/cm]	Density [g/cm^3]	Silver content [%]	Silver powder particles size range [nm]
600n	4.0–5.5	33	0.9–1.1	20	20–100
60n	5.0–6.5	35	0.8–1.0	20	20–100
6n	7.5–10.5	28.5–32.5	1.1–1.3	45	3–8

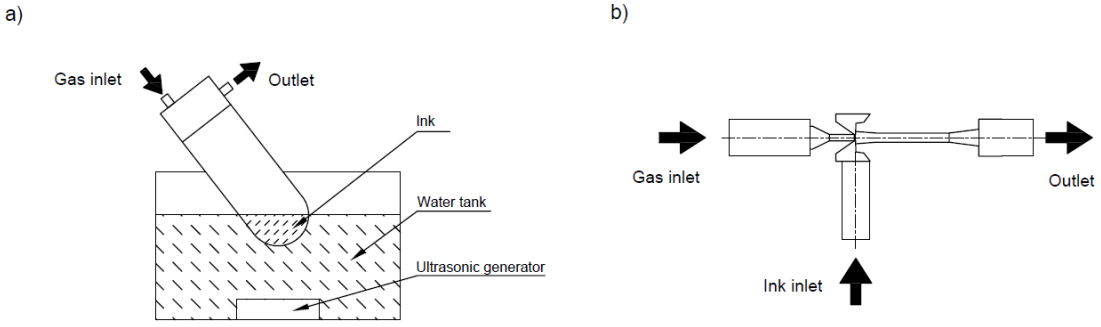


Fig. 2. Schematics of generators: **(A)** ultrasonic and **(B)** pneumatic

Poland). The selection of inks with various properties enabled a precise comparison of the aerosols generated. All the properties are given in Table 1. Aerosol particles were transported through a 250 mm long pneumatic hose and deposited on a polyethylene terephthalate (PET) with a thickness of 200 µm. PET is considered to be one of the most suitable polymer materials for flexible electronics applications because of its high resistance to tearing and humidity compared with that of paper and its lower price in comparison to high-temperature-resistant polyimide [22].

The two aerosol generators used in the research are shown in Figure 2. The first generator utilizes a piezoelectric transducer that generates ultrasonic waves at the surface. In this technique, the liquid is frequently enclosed in a container surrounded by water. Droplets are generated inside the container at a specific height over the transducer. Gas given at the outlet has a role in carrying aerosol further into the nozzle, but has no role in droplet generation. During the AJP process, the ink is heated by acoustic waves; therefore, water is used to cool the container. The rise in temperature has a negative impact on the stability of the process, leading to rapid evaporation of the liquid phase and the parameters of the ink. The pneumatic generator, on the other hand, has constant feed of the liquid which is atomized by the flow of the carrier gas. The difference between the pressures of the gas at the inlet and the liquid inside the container leads to suction of the ink into the generator. The high flow is responsible for tearing off and breaking down into separate small droplets. In a pressure generator, the liquid is not heated, more viscous liquids can be used, and the process is more stable over time. Ultrasonic generation is monodisperse, and for pneumatic generation, it is necessary to maintain the monodispersity of the generated aerosol.

The pressures for both generators were empirically determined. For a pneumatic generator, it is a minimal value of pressure for which aerosol formation occurs due to ligament detachment and for an ultrasonic for which transportation of aerosol droplets into the process is possible. The pressures used for the pneumatic generator are too high for the AJP process. With increasing pressure, a reduction in aerosol DD is observed. The generation is strictly tied to the pressure flowing through the spray nozzle (Figure 2B). Greater pressure of the carrier gas causes the formation of longer ligaments, which then break down into droplets of smaller diameters. As a result of the combination of process and pressure, it becomes problematic to

Table 2. Pressures used for the ultrasonic (a) and pneumatic (b) generator

Ink	**Pressure (mbar)**												
(a)													
6n	50	60	70	80	90	100	110	120	130	140	150		
60n				80	90	100	110	120	130	140	150		
600n						100	110	120	130	140	150		
(b)													
6n	600	700	800	900	1,000	1,100	1,200	1,300	1,400	1,500	1,800	2,000	2,500
60n	600	700	800	900	1,000	1,100	1,200	1,300	1,400	1,500	1,800	2,000	2,500
600n	600	700	800	900	1.000	1.100	1.200	1.300	1.400	1.500	1.800	2.000	2.500

generate an aerosol for lower pressures. For this purpose, the Virtual Impactor is used; it allows you to get rid of excess pressure and, with appropriate design, also to select the droplet size, which directly affects the monodispersity of the aerosol (Figure 6A) In the case of an ultrasonic generator, the aerosol formation process itself is independent of pressure, but the parameters may change over time as the suspension heats up. However, as the applied pressure increases, the droplet size increases (Figure 6B). This happens because of the pressure needed to transport droplets with a larger mass.

The pressures were gradually changed by 10 mbar for the ultrasonic generator and 100 mbar for the pneumatic generator. Furthermore, after reaching 1,500 mbar for the pneumatic generator, the sequence 1,800 mbar, 2,000 mbar, and 2,500 mbar were chosen to examine the influence of higher pressure on aerosol droplet formation. The parameters are collected and shown in Table 2. Within the selected range, a precise analysis was possible. The lowest pressure values initiated generation and transport of the aerosol, while with the highest values, deposited droplets of aerosol started to unite on the substrate surface. Compressed air was used as the carrier gas. For a precise pressure dosage, a piezoelectric pump was used (Elveflow OB1 MK3+, Paris, France).

A reliable analysis was possible due to the combination of three different inks with two types of generators. As a result, the influence of ink parameters and the characteristic of the generator on the formed aerosol were recognized.

The morphology of the generated particles was measured in the deposited state to compare the influence of the ink properties on the spreadability and ability to overspray formation. The VHX-6000 digital microscope (Keyence, Osaka, Japan) was applied to analyze the droplets generated and deposited according to the ISO 16232 standards (Figure 3A and 3B). When the image (Figure 3A) is divided into multiple regions and each region is individually analyzed, the "special measurement" function allows users to perform a contamination analysis over a large area. The analysis displays the number of detected particles and the cleanliness level for each maximum diameter class. Ten pictures were captured using a magnification of 300× for each ink aerosol formed by each generator. As a result, the algorithm displayed diagrams with distribution of the particles with specified diameter (Figure 3B). As every image is stored as separate spreadsheets it is needed to be exported and stored using dynamic tables. Due to an immense level of data, different types of representations have been examined. A significant part of the data was not falling into normal distribution; due to this problem commonly used tools for statistics could be blurring information from the data. To compare different datasets, box plot with whiskers was used instead of the bar graph, and this representation shows condensate data in one plot. Corresponding quantiles, median and interquartile range (IQR), were calculated for each of the pressures. The whiskers in the plot are 1.5 IQR, where IQR is defined as the difference between the third and first quartiles. Outliers were marked with bars exceeding 1.5 IQR zone, and due to large dataset, separate points would be hard to read.

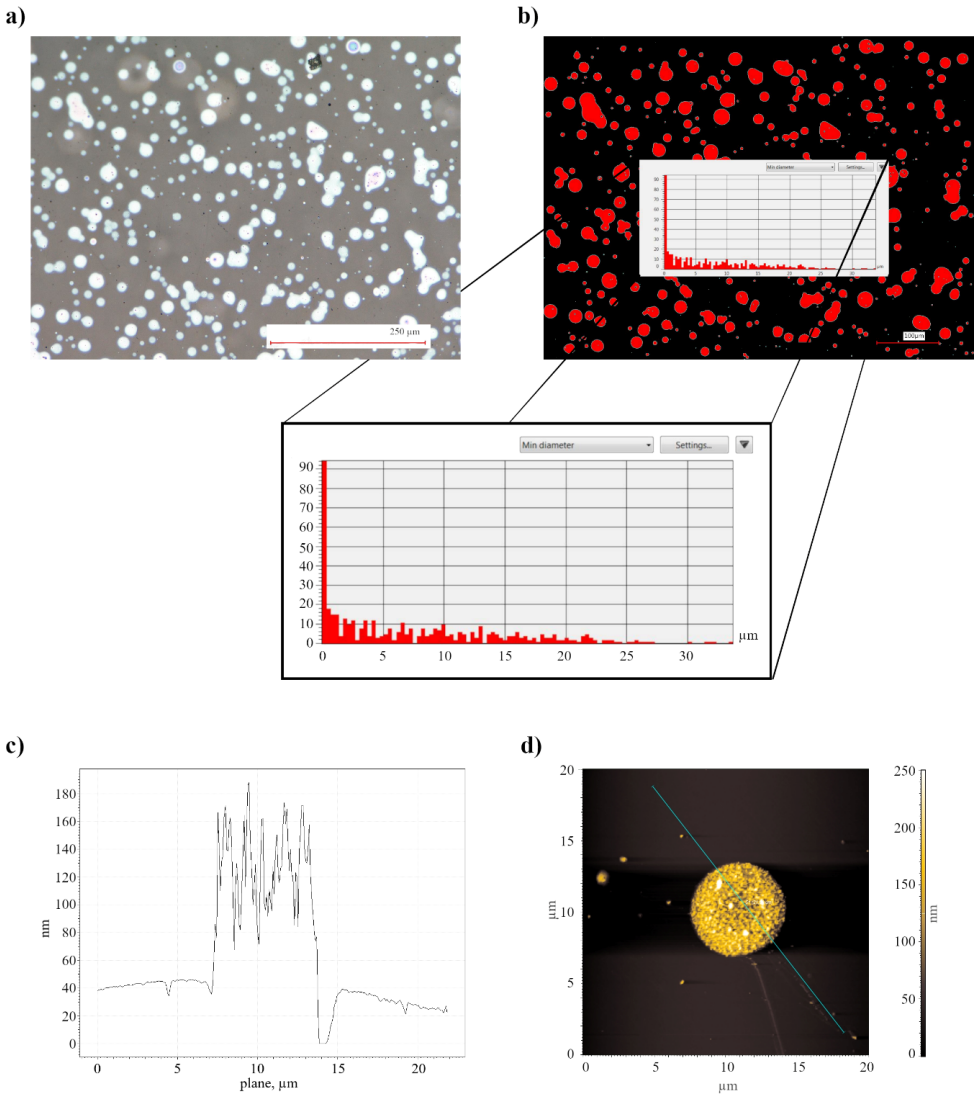


Fig. 3. Exemplary measurement: **(A)** photo from digital microscope, **(B)** measurement of the droplets size, **(C)** cross section of the droplet from AFM, and **(D)** view from above from AFM. AFM, atomic force microscopy

It should be emphasized that ink wettability influences the DD of the aerosol sprayed and depends on the surface tension and interfacial tension of the ink and substrate. Therefore, two laboratory techniques were used to examine the morphology of the deposited droplets by diagnostic scans, that is, scanning electron microscope (SEM) and AFM. The morphology of the deposited droplets was analyzed using a Tescan VEGA 3 SBH SEM equipped with a secondary electron (SE) detector. Prior to analysis, the samples were sputtered with ions of gold to form a 5-nm thin coating and obtain high-quality images despite nonconductive and beam-sensitive polymer substrate. An AFM microscope (NT-MDT NTEGRA Prime, Apeldoorn, The Netherlands) was used to analyze the surface topography and morphology of the deposited droplets to control the formation of an overspray layer. AFM scans were performed with the use of resonant, noncontact mode, and PPP-NCLR NANOSENSORS cantilevers. An example measurement is shown in Figures 3C and 3D.

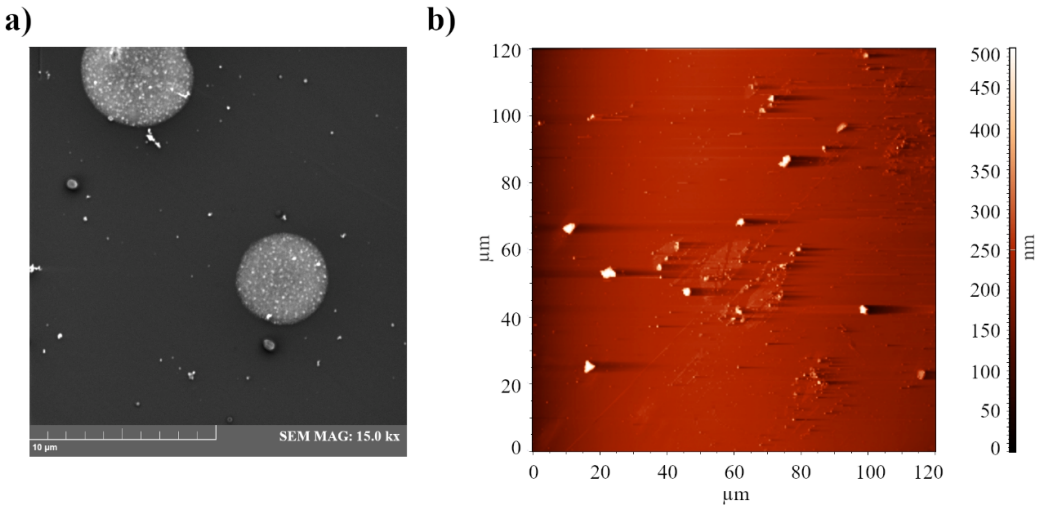


Fig. 4. Images of the droplets below 1 µm from **(A)** SEM and **(B)** AFM. AFM, atomic force microscopy; SEM, scanning electron microscopy

4. Results and discussion

Prior to the precise analysis of the droplet size, the morphology and topography of the deposits was examined. The results showed that a great deal of small droplets with diameter below 1 µm were formed (Figure 4). The appearance of such small droplets depends on the generator and impact energy of the droplets on the substrate surface. First, for the ultrasonic generator, it is reported that smaller droplets, known as satellite droplets, are generated due to interference at the surface of the liquid and the Faraday instability [1]. The next explanation of satellite formation is the generator principle of operation. The ultrasonic waves cause mismatch of the relationship of Reynolds and Weber numbers, similar to ink jet observations [23]. For the pneumatic generator, when the ligaments form larger droplets, they undergo deformation in confinement [24]. Taylor analyzed the deformation of the droplet in the shear flow [25], and proposed a dimensionless number later called capillary number, which is defined as:

$$Ca = \mu a \alpha / \sigma, \tag{4}$$

where μ is viscosity, a is DD, α is shear rate and σ is interfacial tension.

The capillary number defines the ratio between viscosity and capillary forces and strongly influences the aerosol generation process. After reaching the critical value, the droplet occurs. On the other hand, the viscosity ratio affects the breakdown of the droplets and satellite formation [26]. For both methods used, further generation of the satellite droplets occurs together with splashing of the liquid onto the substrate and depends on different parameters, such as: (i) contact angle between the liquid and the substrate [27], (ii) impact velocity and DD [28], (iii) Weber number [29], and (iv) Ohnesorge number [30]. After crossing some velocity value, known as critical velocity, splashing of the droplet takes place. It is worth noting that droplets with larger diameters easily achieve critical velocity [31]. Generally, two types of splashing are distinguished: (i) corona splash and (ii) prompt splash. Corona splashing is the result of lifting the lamella off the surface. Small droplets detach as a result of the lamella break up. In the case of prompt splash, the droplets spread and tiny droplets tear off the nose of the liquid sheet [32]. It is worth noting that for each type of splash the physical mechanism can be different. With increasing carrier gas pressure, prompt splash is more likely to occur [33].

The diameters of the aerosol droplets formed for all inks tested by both are presented in the box plot in Figure 6. The number of droplets deposited with lower pressure of the carrier gas was

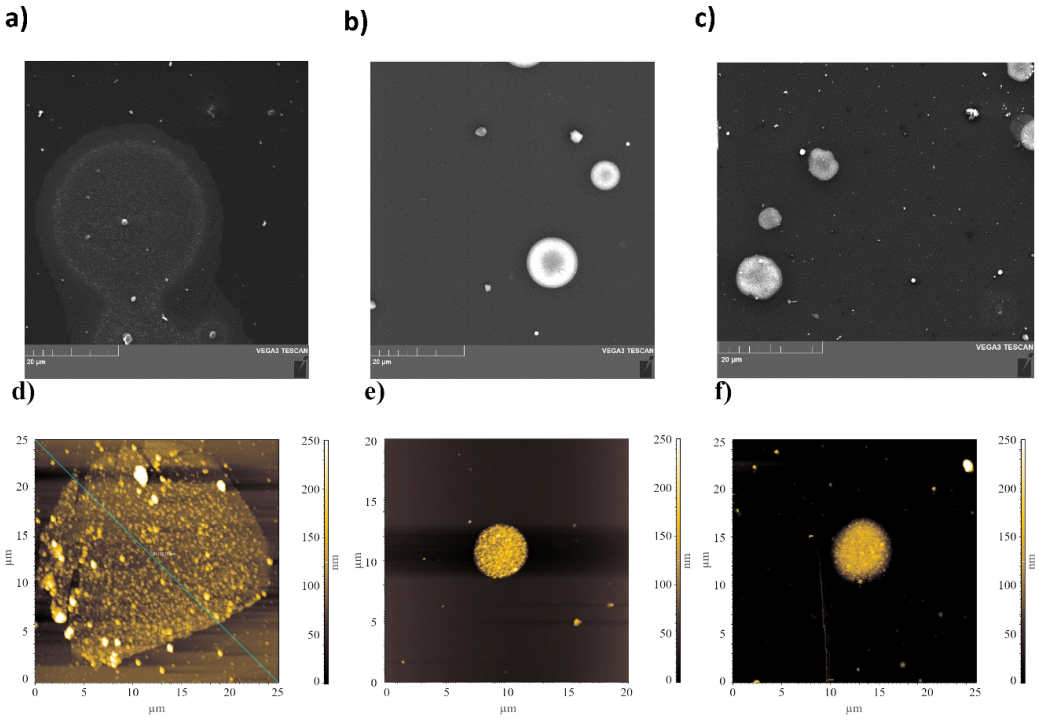


Fig. 5. SEM images for pneumatic generator 1,800 mbar: **(A)** 6n ink, **(B)** 60n ink, **(C)** 600n ink, AFM images for ultrasonic generator 150 mbar, **(D)** 6n ultrasonic, **(E)** 60n ultrasonic, and **(F)** 600n ultrasonic. AFM, atomic force microscopy; SEM, scanning electron microscopy

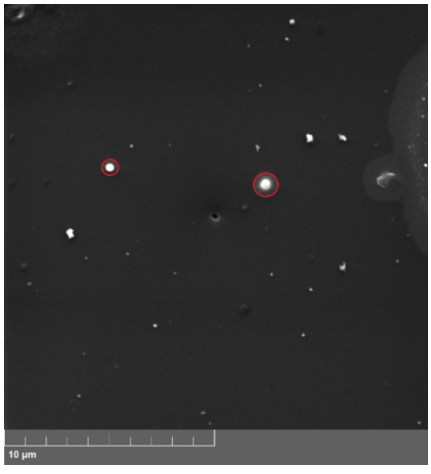


Fig. 6. SEM image for pneumatic generator 1,800 mbar 6n ink. SEM, scanning electron microscopy

insufficient for reliable statistics, independently of the generator type. Therefore, graphs were created only for results obtained with working gas pressures above 110 mbar and 1,200 mbar for the ultrasonic and pneumatic generator, respectively.

In the case of ink 6n, the largest droplet formation is observed independently on the generator used (Figure 5A and 5D). The range of results is also the largest (Figure 7). The relationship between the droplet size and the carrier gas pressure for ultrasonic generators is direct. Increasing the pressure of the working gas increases DD. The formed droplets are weakly packed with silver nanoparticles compacted in agglomerates and scattered in the spread area. Furthermore, some satellite droplets with relatively high density were detected. In the case of a pneumatic generator, the relationship is inversely proportional, and thus DD decreases with increased gas pressure. In addition, the drop region is divided into two areas: (i) the first with visible silver nanoparticles and (ii) the second with spilled solvent. In some of the smaller droplets, a similar solvent spill effect may be seen (Figure 6 red circles). However, the compactness of the silver nanoparticles is significantly higher. The second area is created due to the spreading and receding of the droplet after impact [34].

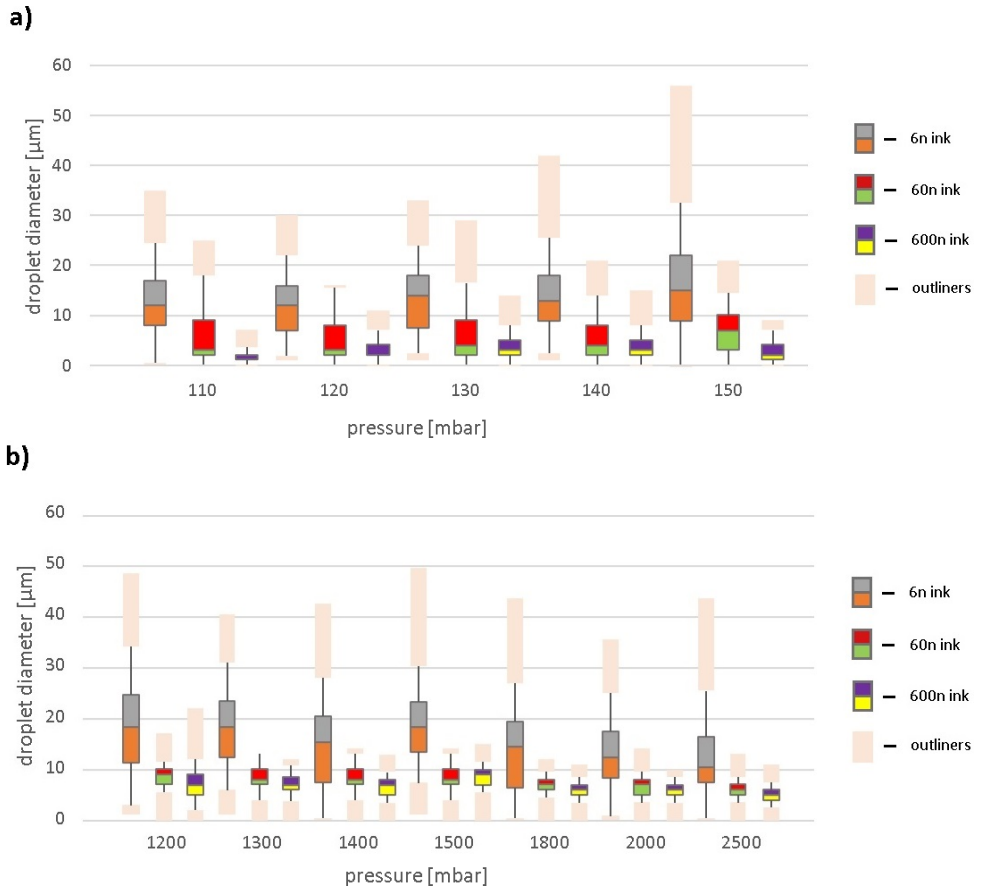


Fig. 7. Box plot of measured droplets for **(A)** ultrasonic generator and **(B)** pneumatic generator

In the case of ink 60n, the DD are smaller compared with ink 6n (Figure 7A and 7B). The data for the ultrasonic generator presented in Figure 7 show positive skewness, which decreases with increasing pressure. However, the bars in the primary data of the histogram representation have a shape of exponential distribution (exemplary histogram shown in Figure 3B). It induces problems for commonly used statistical tools such as mean diameter or normal deviation, which are more related to normal distribution. In addition, whiskers and outliers have high value. The droplets generated by ultrasonics indicated the presence of agglomerates (see Figure 5E). Compared with ink 6n, those agglomerates are smaller and denser; simultaneously, they contain more silver particles, whereas the droplet areas are scattered more evenly. The IQR data for pneumatic generator is more monodisperse. The larger droplets generated by the pneumatic system tend to change shape leaving less material in the middle of the deposit (Figure 5B).

Ink 600n showed the smallest DD of all inks produced by both pneumatic and ultrasonic generators (Figure 7). Especially efficient appeared to be the ultrasonic generator with positive skewness, and up to 67% of droplets with 1 µm diameter were obtained for 110 mbar of carrier gas. Analogous to 60n ink data, the 600n primary data histogram representation has exponential distribution with even steeper slope. The droplets produced by the ultrasonic generator are the most dense compared with other inks (Figure 5F). On the other hand, pneumatically generated DD of the 60n and 600n inks are comparable (Figure 7). However, the droplets have less material in the middle and their shape is repeatedly non-circular (Figure 5C), although small agglomerates inside the droplet can be found for both generators.

On the basis of analysis of the results, it is stated that midair evaporation leads to shell formation on the droplet surface, while the splashing mechanism causes detachment of the droplet into small pieces. Both phenomena are responsible for the scattering, aggregation, and transport of compacted silver nanoparticles outside the drop area [35, 36]. Other mechanisms that influence the morphology of the droplets observed for inks 60n and 600n are related to the migration of nanoparticles inside the droplet. During evaporation, the nanoparticles are dragged to the contact area, creating a ring also called the "coffee stain effect" [37–39]. Analogous effects are reported in inkjet printing [40]. This phenomenon also contributes to the creation of "doughnut"-shaped droplets [41], which are presented in Figure 5B).

Analysis of three types of inks clearly showed that the dynamic viscosity most significantly influences the diameters of the aerosol droplets. The dynamic viscosity of the liquid describes its resistance to flow when an external force is applied, which means the resistance to movement of one layer of a fluid over another [42, 43]. Therefore, the separation of viscous ink into droplets was hindered. Similar results were obtained by Heng et al. [44] who generated solid phase aerosols from viscous solutions or suspensions and found that the increase in velocity in the range from 4 cSt to 39 cSt caused a modest increase in the median aerodynamic diameter. On the other hand, low viscosities usually lead to satellite formation. However, other liquid properties, such as surface tension and density, also influence the morphology of aerosol droplets [45, 46]. Kwon measured drop formation curve in the drop-on-demand (DOD) process and found that high surface tension can prevent the formation of satellite droplets [47]. It is worth emphasizing that the ink properties can be regulated and even changed by applied generator. It is clearly visible in Figure 6, that independently of the ink used, the ultrasonic generator formed particles with a smaller diameter. Lin et al. [48] analyzed the piezoelectric inkjet aerosol generator and concluded that the appropriate combination of parameters allows the production of a liquid aerosol with rheological properties similar to those of water [48]. In addition, the authors applied air dispersion to reduce coagulation. The same treatment was done in this study using a higher pressure in the pneumatic generator to prevent coupling of small aerosol droplets. However, the smaller size of droplets obtained by the ultrasonic generator may result from additional heating of the ink and liquid vaporization. Long-term heating of the medium causes its drying and problems with perseverance of the stable parameters in time [11].

When comparing two generators, it is stated that pneumatic is a promising variation. It provides a more stable process over time, and there is no problem with undesirable heating. Furthermore, operating at higher pressure allows us to develop a system compatible with the Virtual Impactor. The application of a Virtual Impactor allows reducing the pressure at the input of the AJP nozzle, and by acting on lifting forces to reduce satellite droplets, thus reducing overspray [49, 50]. For an ultrasonic generator, such a solution is not available [51]. An increase in pressure could lead to a deviation of the DD. Furthermore, ultrasounds have limited efficiency. When the optimum value of the carrier gas pressure is exceeded, the density of aerosol droplets in the carrier gas volume decreases significantly. Increasing the voltage applied to the generator does not solve the problem, due to increased overheating and further destabilization of the process. Moreover, the pneumatic generator is more stable and insensitive for the properties of the ink optimization parameters, reducing the issue of additional parameters after the ink is changed. The remaining problem is the agglomeration of silver particles within the droplet. Further research with deposited ink film should be provided to address this issue.

5. Conclusions

In this study, three types of ink were used in combination with ultrasonic and pressure generators to fabricate aerosols. Ink parameters, as well as generation method, influenced aerosol behavior and DD. Droplets fabricated by ultrasonic and pneumatic generators were sprayed through the outlet hose on the PET foil. The following conclu-

sion can be drawn from the study:

1. The type of generator and ink properties influence the size of the droplets. The relationship between the droplet size and the carrier gas pressure for the ultrasonic generator was proportional, whereas for the pneumatic generator it was inversely proportional. However, many small droplets with diameter below 1 µm were formed.
2. Regardless of the ink used, the DD decreased with increasing pressure of the working gas in the pneumatic generator. Furthermore, the inks with a dynamic viscosity below 6.5 $m \cdot Pa^{-1} \cdot s^{-1}$ maintain the diameter in the stable range of 5–10 µm, regardless of the working gas pressure. However, the presence of dense agglomerates with satellite droplets was observed with the highest pressure of the carrier gas. The size of the aerosol particles depends on the capillary number and arises from the deformation of the droplets.
3. Despite the significantly lower working pressure, the ultrasonic generator easily increased the size of the fed droplets with increasing pressure of the carrier gas. Moreover, the diameter of the droplets significantly decreased from 7–22 µm to 1–5 µm with a reduction in the dynamic viscosity of the inks from 7.5–10.5 $m \cdot Pa^{-1} \cdot s^{-1}$ to 4–5.5 $m \cdot Pa^{-1} \cdot s^{-1}$, respectively. Ultrasonic waves cause a Faraday instability as well as a mismatch of the relationship of Reynolds and Weber numbers, which increases the range of particles size and simultaneously causes satellite formation.
4. The influence of the ink properties on the droplets size was observed. A high viscosity ink of 7.5–10.5 $m \cdot Pa^{-1} \cdot s^{-1}$ produced the largest aerosol droplets, mostly in the range of 7–22 µm and 6–25 µm, for ultrasonic and pneumatic generator, respectively. However, the density of the deposited silver nanoparticles is lower due to the spill effect of the impacting droplet. Droplets of lower dynamic viscosity inks (below 6.5 $m \cdot Pa^{-1} \cdot s^{-1}$) tend to change shape as a result of impact, leaving less material in the middle of the deposit and forming the shape of a doughnut. This effect is particularly noticed with the use of a pneumatic generator. Nevertheless, the density of formed droplets and agglomerates is higher.
5. The final size of the deposited droplet depends on the splashing of the liquid on the substrate, while the most crucial factors are the size of the droplets, Weber and Ohnesorge numbers, the contact angle, and the impact velocity. Therefore, future research should focus on application of the inks in the AJP process with dedicated two channel sheath/carrier gas nozzles and evaluation of the overspray region.

Funding

This work was funded by the National Centre of Research and Development [**LIDER/42/0142/L-11/19/NCBR/2020]** (Project title: Sonic Jet – precise printer for manufacturing elastic electronics)

Conflict of interest

The authors declare that they have no known competing financial interests or personal relationships that could have appeared to influence the work reported in this paper.

References

[1] Kooij S, Astefanei A, Corthals GL, Bonn D. Size distributions of droplets produced by ultrasonic nebulizers. *Sci Rep*. 2019;9:6128. doi:10.1038/s41598-019-42599-8.

[2] Mitchell J, Nagel M. Particle size analysis from medicinal inhalers. *KONA Powder Part J*. 2004;22: 32–5. doi:10.14356/kona.2004010.

[3] Aghajani S, Accardo A, Tichem M. Process and nozzle design for high-resolution dry aerosol direct writing (dADW) of sub-100 nm nanoparticles. *Addit Manuf*. 2022;54: 102729. doi:10.1016/j.addma.2022.102729.

[4] Gou Y, Jia Y, Wang P, Sun C. Progress of inertial microfluidics in principle and application. *Sensors (Basel)*. 2018;18: 1762. doi:10.3390/s18061762.

[5] Di Carlo D. Inertial microfluidics. *Lab Chip*. 2009;9: 3038–46. doi:10.1039/b912547g.

[6] Chen G, Gu Y, Tsang H, Hines DR, Das S. The effect of droplet sizes on overspray in aerosol-jet printing. *Adv Eng Mater*. 2018;20, 1701084. doi:10.1002/adem.201701084.

[7] Saffman PG. The lift on a small sphere in a slow shear flow. *J Fluid Mech*. 1965;22: 385–400.

[8] Rühle F, Schaaf C, Stark H. Optimal control of colloidal trajectories in inertial microfluidics using the Saffman effect. *Micromachines (Basel)*. 2020;11: 592. doi:10.3390/MI11060592.

[9] Akhatov IS, Hoey JM, Swenson OF, Schulz DL. Aerosol focusing in micro-capillaries: theory and experiment. *J Aerosol Sci*. 2008;39: 691–9. doi:10.1016/j.jaerosci.2008.04.004.

[10] Tafoya RR, Secor EB. Understanding effects of printhead geometry in aerosol jet printing. 2020, 5, 035004

[11] Hoey JM, Lutfurakhmanov A, Schulz DL, Akhatov IS. A review on aerosol-based direct-write and its applications for microelectronics. *J Nanotechnol.* 2012, 324380. doi:10.1155/2012/324380.

[12] Secor EB. Principles of aerosol jet printing. *Flex Print Electron*. 2018;3. 03502 doi:10.1088/2058-8585/aace28.

[13] Rajan R, Pandit AB. Correlations to predict droplet size in ultrasonic atomisation. *Ultrasonics*. 2001;39(4): 235–55. doi:10.1016/s0041-624x(01)00054-3.

[14] Lang RJ. Ultrasonic atomization of liquids. *J Acoust Soc Am*. 1962;34,6-8

[15] Lozano A, García JA, Alconchel J, Barreras F, Calvo E, Santolaya JL. Influence of liquid properties on ultrasonic atomization. ILASS–Europe 2017, 28th Conference on Liquid Atomization and Spray Systems, 6-8 September 2017, Valencia, Spain; doi:10.4995/ilass2017.2017.4588.

[16] Barreras F, Amaveda H, Lozano A. Transient high-frequency ultrasonic water atomization. *Exp Fluids*. 2002;33: 405–13. doi:10.1007/s00348-002-0456-1.

[17] Villermaux E. Fragmentation. *Annu Rev Fluid Mech*. 2007;39: 419–46. doi:10.1146/annurev.fluid.39.050905.110214.

[18] Shardt N, Wang Y, Jin Z, Elliott JAW. Surface tension as a function of temperature and composition for a broad range of mixtures. *Chem Eng Sci*. 2021;230: 116095. doi:10.1016/j.ces.2020.116095.

[19] Petravic J, Delhommelle J. Hydrogen bonding in ethanol under shear. *J Chem Phys*. 2005;122: 234509. doi:10.1063/1.1940050.

[20] Gañán-Calvo AM. Generation of steady liquid microthreads and micron-sized monodisperse sprays in gas streams. 1998, 80, 2-12 doi: 10.1103/PhysRevLett.80.285

[21] Ohnesorge WV. Die Bildung von Tropfen an Düsen und die Auflösung flüssiger Strahlen. *Zeitschrift Für Angewandte Mathematik Und Mechanik*. 1936;16: 355–8. doi:10.1002/zamm.19360160611.

[22] Yakimets I, MacKerron D, Giesen P, Kilmartin KJ, Goorhuis M, Meinders E, et al. Polymer substrates for flexible electronics: achievements and challenges. *Adv Mat Res*. 2010;93–94: 5–8. doi:10.4028/www.scientific.net/AMR.93-94.5.

[23] Zhang Y, Hu G, Liu Y, Wang J, Yang G, Li D. Suppression and utilization of satellite droplets for inkjet printing: a review. *Processes*. 2022;10: 932. doi:10.3390/pr10050932.

[24] Ioannou N, Liu H, Zhang YH. Droplet dynamics in confinement. *J Comput Sci*. 2016;17: 463–74. doi:10.1016/j.jocs.2016.03.009.

[25] Taylor GI. The formation of emulsions in definable fields of flow. *Proceedings of the Royal Society of London Series A, Containing Papers of a Mathematical and Physical Character*. 1934;146: 501–23. doi:10.1098/rspa.1934.0169.

[26] Sibillo V, Pasquariello G, Simeone M, Cristini V, Guido S. Drop deformation in microconfined shear flow. *Phys Rev Lett*. 2006;97: 054502. doi:10.1103/PhysRevLett.97.054502.

[27] Yokoi K. Numerical studies of droplet splashing on a dry surface: triggering a splash with the dynamic contact angle. *Soft Matter*. 2011;7: 5120–3. doi:10.1039/c1sm05336a.

[28] Motzkus C, Gensdarmes F, Géhin E. Parameter study of microdroplet formation by impact of millimetre-size droplets onto a liquid film. *J Aerosol Sci*. 2009;40: 680–92. doi:10.1016/j.jaerosci.2009.04.001.

[29] Yonemoto Y, Tashiro K, Shimizu K, Kunugi T. Predicting the splash of a droplet impinging on solid substrates. *Sci Rep*. 2022;12,5093. doi:10.1038/s41598-022-08852-3.

[30] Motzkus C, Gensdarmes F, Géhin E. Study of the coalescence/splash threshold of droplet impact on liquid films and its relevance in assessing airborne particle release. *J Colloid Interface Sci*. 2011;362: 540–52. doi:10.1016/j.jcis.2011.06.031.

[31] Stow CD, Hadfield MG. An experimental investigation of fluid flow resulting from the impact of a water drop with an unyielding dry surface. 1981;373, 1755, 419-441 doi: 10.1098/rspa.1981.0002.

[32] Almohammadi H, Amirfazli A. Droplet impact: viscosity and wettability effects on splashing. *J Colloid Interface Sci*. 2019;553: 22–30. doi:10.1016/j.jcis.2019.05.101.

[33] Latka A, Strandburg-Peshkin A, Driscoll MM, Stevens CS, Nagel SR. Creation of prompt and thin-sheet splashing by varying surface roughness or increasing air pressure. *Phys Rev Lett*. 2012;109: 054501. doi:10.1103/PhysRevLett.109.054501.

[34] Ebrahim M, Ortega A. Identification of the impact regimes of a liquid droplet propelled by a gas stream impinging onto a dry surface at moderate to high weber number. *Exp Therm Fluid Sci*. 2017;80: 168–80. doi:10.1016/j.expthermflusci.2016.08.019.

[35] Mezhericher M, Levy A, Borde I. Modelling the morphological evolution of nanosuspension droplet in constant-rate drying stage. *Chem Eng Sci*. 2011;66: 884–96. doi:10.1016/j.ces.2010.11.028.

[36] Woźniak M, Derkachov G, Kolwas K, Archer J, Wojciechowski T, Jakubczyk D, et al. Formation of highly ordered spherical aggregates from drying microdroplets of colloidal suspension. *Langmuir*. 2015;31: 7860–8. doi:10.1021/acs.langmuir.5b01621.

[37] Deegan RD. Pattern formation in drying drops. *Am Phys Soc*. 2000;60: 475–85.

[38] Deegan RD, Bakajin O, Dupont TF, Huber G, Nagel SR, Witten TA. Contact line deposits in an evaporating drop. *Am Phys Soc*. 2000;62: 756–65.

[39] Deegan RD, Bakajin O, Dupont TF, Huber G, Nagel SR, Witten TA. Capillary flow as the cause of ring stains from dried liquid drops. *Nature*. 1997;389: 827–9. doi:10.1038/39827.

[40] Ikegawa M, Azuma H. Droplet behaviors on substrates in thin-film formation using ink-jet printing. *JSME Int J*. 2004;47: 490–6.

[41] Wang J, Evans JRG. Drying behaviour of droplets of mixed powder suspensions. *J Eur Ceram Soc*. 2006;26: 3123–31. doi:10.1016/j.jeurceramsoc.2005.08.018.

[42] Soares C. Gas turbine fuel systems and fuels. In: *Gas turbines*. Elsevier; Dallas, 2015, p.317–411. doi:10.1016/B978-0-12-410461-7.00007-9.

[43] Martyr AJ, Rogers DR. Chapter 15 – Measurement of liquid fuel, oil, and combustion air consumption. *Engine Testing*. 2021;5: 511–35. doi:10.1016/B978-0-12-821226-4.00015-2.

[44] Heng X, Yeates DB. Generation of high concentrations of respirable solid-phase aerosols from viscous fluids. *Aerosol Sci Technol*. 2018;52: 933–52. doi:10.1080/02786826.2018.1488078.

[45] Shimoda T, Morii K, Seki S, Kiguchi H. Introduction: the microliquid process. *MRS Bull*. 2003;28: 821–7.

[46] Xiao X, Li G, Liu T, Gu M. Experimental study of the jetting behavior of high-viscosity nanosilver inks in inkjet-based 3d printing. *Nanomaterials (Basel)*. 2022;12: 3076. doi:10.3390/nano12173076.

[47] Kwon KS. Experimental analysis of waveform effects on satellite and ligament behavior *via in situ* measurement of the drop-on-demand drop formation curve and the instantaneous jetting speed curve. *J Micromech Microeng*. 2010;20: 115005. doi:10.1088/0960-1317/20/11/115005.

[48] Lin CW, Kuo TH, Huang SH, Kuo YM, Wu WJ, Chen CC. Characterization of a piezoelectric inkjet aerosol generator for the study of bioaerosol survivability. *Aerosol Air Qual Res*. 2019;19: 959–70. doi:10.4209/aaqr.2018.07.0254.

[49] Reitelshöfer S, Göttler M, Schmidt P, Treffer P, Landgraf M, Franke J. Aerosol-jet-printing silicone layers and electrodes for stacked dielectric elastomer actuators in one processing device. In: *Proceeding of SPIE 9798, Electroactive Polymer Actuators and Devices (EAPAD) 2016, 15 April 2016*; 2016, p.97981Y. doi:10.1117/12.2219226.

[50] Chen BT, Yeh HC. An improved virtual impactor: design and performance. *J Aerosol Sci*. 1987;18: 203–14. doi:10.1016/0021-8502(87)90056-5.

[51] Gupta AA, Bolduc A, Cloutier SG, Izquierdo R. *2016 IEEE International Symposium on Circuits and Systems (ISCAS)*. IEEE; 2016.

Received 2022-12-07
Accepted 2023-02-20